Supplementary material to "Quantum dot single-photon sources for entanglement enhanced interferometry"

M. Müller,[1,*] H. Vural,[1] C. Schneider,[2] A. Rastelli,[3]
O. G. Schmidt,[4] S. Höfling,[2,5] and P. Michler[1,†]

[1]*Institut für Halbleiteroptik und Funktionelle Grenzflächen, Center for Integrated Quantum Science and Technology (IQST) and SCoPE, Universität Stuttgart, Allmandring 3, 70569 Stuttgart, Germany*

[2]*Technische Physik and Wilhelm Conrad Röntgen Research Center for Complex Material Systems, Physikalisches Institut, Universität Würzburg, Am Hubland, 97074 Würzburg, Germany*

[3]*Institute of Semiconductor and Solid State Physics, Johannes Kepler University Linz, Altenbergerstrasse 69, 4040 Linz, Austria*

[4]*Institute for Integrative Nanosciences, IFW Dresden, Helmholtzstr. 20, 01069 Dresden, Germany*

[5]*SUPA, School of Physics and Astronomy, University of St. Andrews KY 16 9SS, Scotland, United Kingdom*

(Dated: March 17, 2017)

QUANTUM DOT SAMPLES

Two different samples were investigated to obtain the results presented in this letter. Both contain self-assembled QDs, grown by molecular beam epitaxy in Stranski-Krastanow mode and applying a partial capping and annealing technique.

Sample A, used for the two-photon excitation experiments, contains a single layer of self-assembled In(Ga)As quantum dots in a planar λ-cavity formed by a bottom distributed Bragg reflector (DBR) made up of 15 pairs of $\lambda/4$ layers of AlAs/GaAs and one single pair of GaAs/AlAs on the top.

Sample B, used for the pulsed resonance-fluorescence experiments, contains low density ($\sim 2.2 \cdot 10^9$ cm^{-2}) InAs QDs. The lower and upper DBR of the planar GaAs cavity consists of 24 and 5 pairs of $Al_{0.9}Ga_{0.1}AS$/GaAs, leading to a quality factor of $\sim$200. Despite the planar cavity, lens-shaped modulations significantly enhance the extraction efficiency of the device [1]. A δ-doping layer of silicon donors ($\sim 1.8 \cdot 10^{10}$ cm^{-2}) was implemented 10 nm below the QDs to increase the probability of finding charged excitons.

DETERMINISTIC SINGLE-PHOTON GENERATION

Fig. 1 (QD sample A) and Fig. 2 (QD sample B) illustrate the main characteristics of the deterministically operated single-photon sources.

Due to a different Coulomb interaction between the individual particles of the X and XX, the energies of the emitted photons differ by the XX binding energy (2.3 meV), as shown in the emission spectrum in Fig. 1 (a). This allows for two-photon optical excitation [2–5] (TPE), in which the laser energy is set precisely in between the quantum dot (QD) spectral lines to hit the two-photon resonance of the biexciton state. Various methods were applied to fully remove the scattered laser light from the detector. As expected from the cascaded decay process, both spectral lines have almost equal intensity and moreover no other emission from the sample was detected across a wide spectral range. Fig. 2 (a) shows the spectrum of the resonant pumped T state [6–9]. In contrast to the TPE, spectral filtering is not possible in this case and cross-polarization suppression of the excitation laser is inevitable.

The very selective resonant excitation processes facilitates extremely pure single-photon generation by the individual transitions, as evident from the second-order autocorrelation

measurement of the XX and T photons depicted in Fig. 1 (b) and Fig. 2 (b). The coincidence pattern for the latter is a consequence of a double pulse excitation with a pulse separation of $\sim 4.4\,\mathrm{ns}$. Similar degree of purity was observed for the X photons (not shown here).

Additionally, the resonantly driven ground state–biexciton and ground state–trion systems experience Rabi rotations of the state occupation probabilities, monitored by the photoluminescence intensity, as a function of the excitation strength (see Fig. 1 (c) and Fig. 2 (c)). In a pulsed measurement, this quantity is given by the pulse area which in turn is proportional to the square root of the incident excitation power. Apart from the highly pronounced oscillation, the measurement clearly shows a maximum of state preparation, the so called π-pulse, which was the working point for all measurements presented in the this work. Under these conditions, the coherently and resonantly driven QDs act as deterministic single-photon sources of high purity.

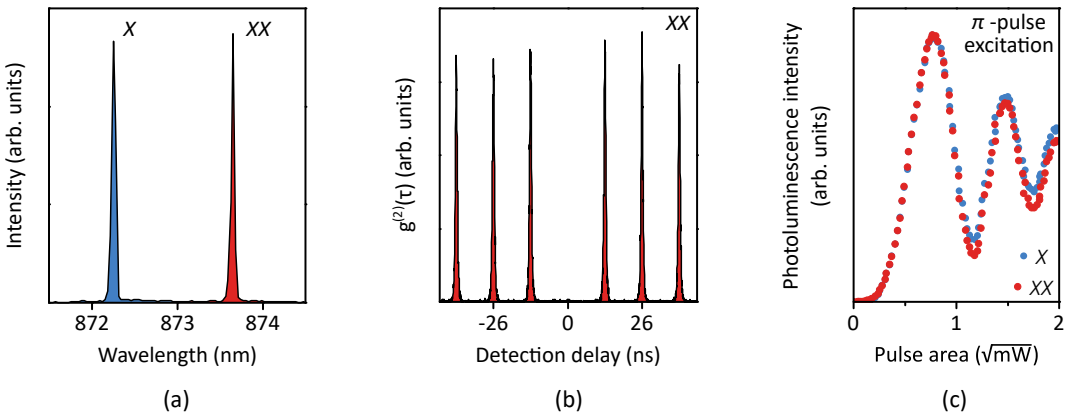

FIG. 1. (a) Emission spectrum in resonant two-photon excitation. The pulsed laser, energetically sitting exactly in between X and XX is completely suppressed. (b) Second-order autocorrelation of XX photons showing pure single-photon emission. The same holds for the X photons (not shown here). (c) X and XX state preparation. Highly pronounced Rabi rotations demonstrate the coherence of the excitation mechanism. All measurements are carried out at the π-pulse, the maximum of the state preparation probability.

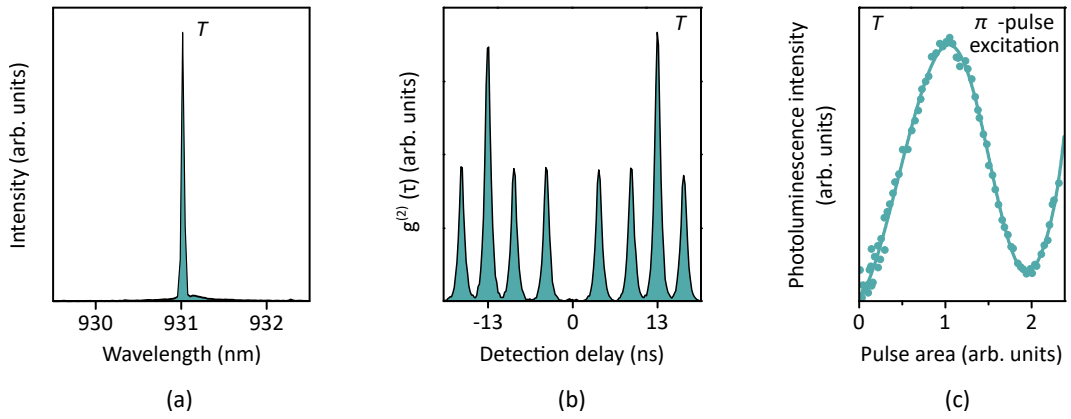

FIG. 2. (a) Emission spectrum in pulsed resonance fluorescence of the T. (b) Second-order autocorrelation of T photons showing pure single-photon emission (double pulse excitation mechanism). (c) T state preparation. Rabi rotations prove the coherence of the process. All measurements are carried out at the π-pulse, ensuring on-demand operation of the single-photon source.

THEORETICAL DESCRIPTION

The theoretical modeling of the Mach-Zehnder operation for different state inputs was derived by combining the basic transformations of the beam splitter operator $\hat{B}$ (with $T = R = 0.5$), phase operator $\hat{\varphi}$ and the operator $\hat{\eta}$ for beam overlap consideration (see below):

$$\hat{B} = \frac{1}{\sqrt{2}} \begin{pmatrix} 1 & \mathrm{i} \\ \mathrm{i} & 1 \end{pmatrix}, \quad \hat{\varphi} = \begin{pmatrix} \mathrm{e}^{\mathrm{i}\varphi} & 0 \\ 0 & 1 \end{pmatrix}, \quad \hat{\eta} = \begin{pmatrix} \sqrt{\eta} & \mathrm{i}\sqrt{1-\eta} \\ \mathrm{i}\sqrt{1-\eta} & \sqrt{\eta} \end{pmatrix}. \tag{1}$$

Fig. 3 shows a sketch of the complete unfolded pathway of the photons with the respective modes. In the ideal case of perfectly indistinguishable photons ($V_{\mathrm{HOM}} = 1$) and maximum beam overlap ($\eta = 1$), the transformation for the creation operators $\hat{a}^\dagger$ and $\hat{b}^\dagger$ for the modes $|a\rangle$ and $|b\rangle$ looks as follows

$$\hat{a}^\dagger \hat{b}^\dagger |00\rangle \xrightarrow{\hat{B}\hat{\varphi}\hat{B}} \frac{1}{4} \left[-\mathrm{i}(e^{-2\mathrm{i}\varphi} - 1)\hat{e}^\dagger \hat{e}^\dagger + \mathrm{i}(e^{-2\mathrm{i}\varphi} - 1)\, \hat{f}^\dagger \hat{f}^\dagger - 2(e^{-2\mathrm{i}\varphi} + 1)\, \hat{e}^\dagger \hat{f}^\dagger \right] |00\rangle \,. \tag{2}$$

For completely distinguishable photons (indicated by '$\sim$') the following relation applies

$$\hat{a}^\dagger \tilde{b}^\dagger |00\rangle \xrightarrow{\hat{B}\hat{\varphi}\hat{B}} \frac{1}{4} \left[-\mathrm{i}(e^{-2\mathrm{i}\varphi} - 1)\hat{e}^\dagger \tilde{e}^\dagger + i(e^{-2\mathrm{i}\varphi} - 1)\, \hat{f}^\dagger \tilde{f}^\dagger - (e^{-\mathrm{i}\varphi} - 1)^2\, \hat{e}^\dagger \tilde{f}^\dagger - (e^{-\mathrm{i}\varphi} + 1)^2\, \hat{f}^\dagger \tilde{e}^\dagger \right] |00\rangle \,. \tag{3}$$

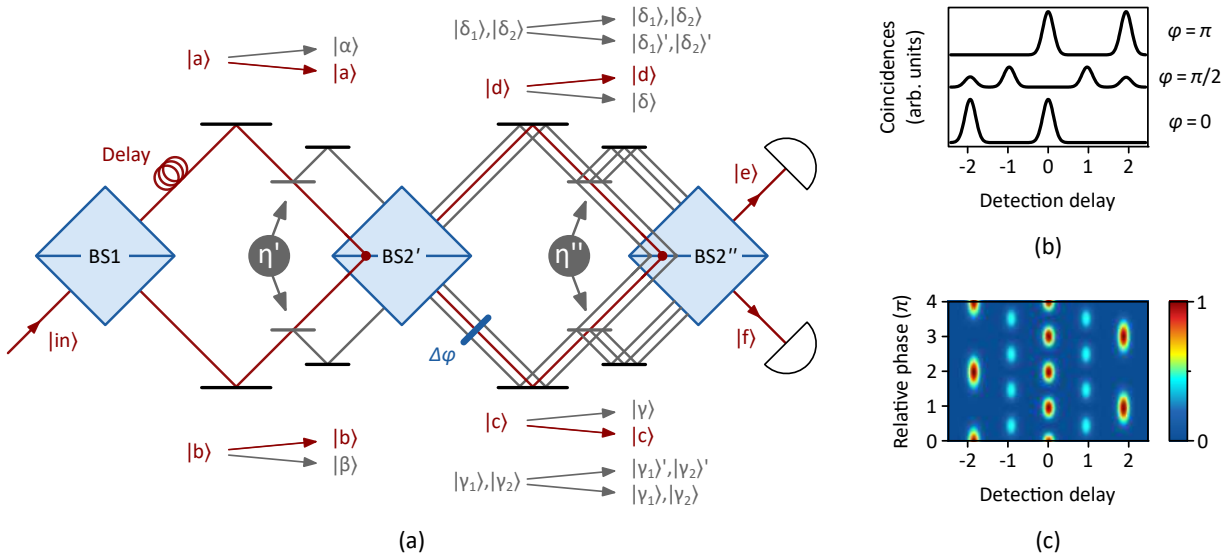

FIG. 3. (a) Schematic of the experimental setup, including all possible spatial modes. η' and η'' correct for non-perfect overlap on BS2′ and BS2″, respectively. The output probabilities are calculated for every possible coincidence combination. (b) Simulated histograms for selected phase settings, ignoring coincidences from consecutive excitation cycles. The well known Hong-Ou-Mandel type five peak pattern is found for odd integer multiples of $\varphi = \pi/2$. Here, entirely indistinguishable photons are assumed, leading to a complete suppression of the middle peak. (c) Simulated phase dependent histograms in a pseudocolor plot. The x-axis is given in units of the time difference between two pulses Δt. Distinct oscillations with single ($\Delta t = \pm 2$) and doubled ($\Delta t = 0, \pm 1$) frequencies are observable. Though, biphotonic N00N-states only contribute to peaks for $\Delta t = 0$, revealing phase super-resolution associated with a true reduction of the de-Broglie wavelength.

The phase dependent coincidence probability is then given by the sum of the individual cases ($\mathcal{P}_{\mathrm{D1,D2}}$ for identical, $\tilde{\mathcal{P}}_{\mathrm{D1,D2}}$ for distinguishable photons), weighted with the indistinguishability visibility $V_{\mathrm{HOM}} = V$:

$$\mathcal{P}^{\mathrm{exp}'}_{\mathrm{D1,D2}} = \underbrace{\frac{V}{2}(1+\cos(2\varphi))}_{\mathcal{P}_{\mathrm{D1,D2}}} + \underbrace{\frac{1-V}{4}(3+\cos(2\varphi))}_{\tilde{\mathcal{P}}_{\mathrm{D1,D2}}} = \frac{1}{4}\left[(3-V)+(1+V)\cos(2\varphi)\right] .$$

For a perfect beam overlap, the reduction of the N00N state contrast strongly depends on the two-photon interference visibility V_{HOM} and is given by $C'_{N=2} = (1+V_{\mathrm{HOM}})/(3-V_{\mathrm{HOM}})$. Spatial modes which do not overlap perfectly are treated as a beam splitter with a $(1-\eta):\eta$ splitting ratio [10]. Here, the reflected modes $|\alpha\rangle$, $|\beta\rangle$ of the operation $\hat{\eta}'$ (gray lines) and

$|\gamma\rangle$, $|\gamma_{1,2}\rangle'$, $|\delta\rangle$, $|\delta_{1,2}\rangle'$ of the operation $\hat{\eta}''$ (purple lines) are feed back into the next BS in the photon path as non-overlapping modes, experiencing only classical correlations. Including this additional non-overlapping contributions, the calculation of the coincidence correlation probability on the detectors D1 and D2 at $\tau = 0$ leads to the phase dependent relation

$$\mathcal{P}^{\mathrm{exp}}_{\mathrm{D1,D2}} = \frac{1}{4}\left(2 + \eta^2(1 - \eta^2 V_{\mathrm{HOM}}) + \eta^2(1 + \eta^2 V_{\mathrm{HOM}})\cos(2\varphi)\right) ,$$

already presented in the main paper. $\eta = \sqrt{\eta'\eta''}$ combines the two individual overlaps on BS2$'$ and BS2$''$, V_{HOM} defines the fraction of utilizable indistinguishable photons.

N00N-STATE INTERFERENCE PATTERN

As already mentioned in the main paper, the two consecutive photons (X, XX or T) arrive with a time separation of $\Delta t = 4.4\,\mathrm{ns}$ at BS1. Because of the 13.1 ns repetition period, coincidence events from photons between different excitation cycles overlap in the histogram. In a theoretical consideration we can remove these additional coincidences and focus on the simple five peak pattern, originating from the statistics obtained by sending a double pulse into an unbalanced Mach-Zehnder interferometer. Fig. 3 (b),(c) show the simulated phase dependent coincidence histograms. For a phase of $\varphi = \pi/2$ the output probabilities of BS2$''$ are identical to the ones obtained after BS2$'$, therefore revealing a typical Hong-Ou-Mandel type histogram. By turning the phase plate the coincidences for all time differences start to oscillate. Besides the double frequently oscillating middle peak for a N00N-state, also the peaks for time differences of $\pm\Delta t$ reveal an oscillating behavior with twice the single photon frequency (Fig. 3 (c)). However, these two photons do not form a N00N-state but travel one by one through the interferometer. Referring to the experimental results, these double frequently occurring $\pm\Delta t$ coincidences are hidden due to the above mentioned overlap of different excitation cycles.

Fig. 4 shows a pseudocolor plot of the measured (left column) and simulated (right column) histograms for X (top row), XX (middle row) and T (bottom row) photons, including the aforementioned coincidence overlaps. The data is very well reproduced by the simulations, and also allows for normalization as shown in Fig. 3 of the main paper.

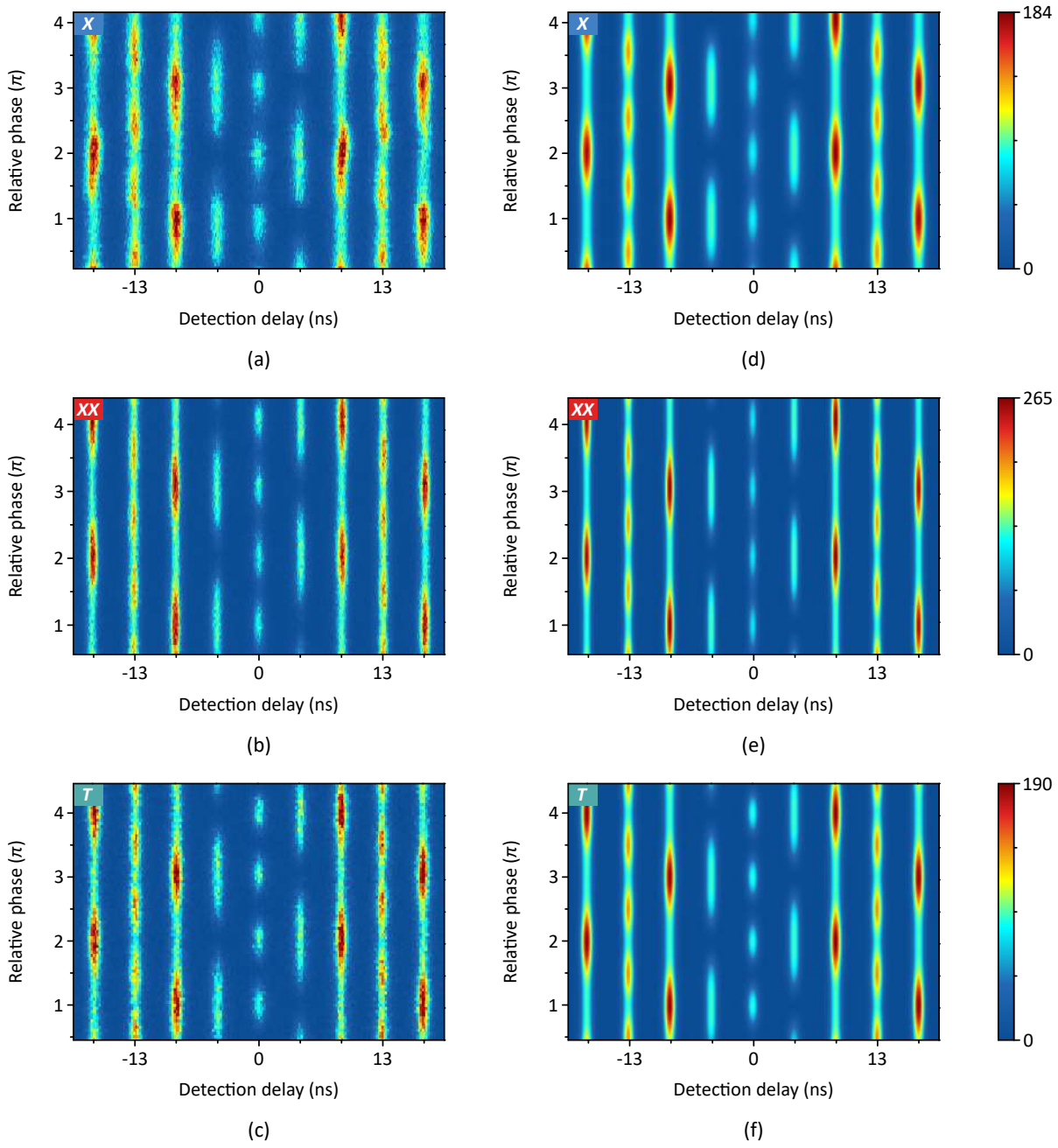

FIG. 4. Complete phase dependence of the measured (a) X, (b) XX and (c) T coincidence histograms. At zero delay, the predicted frequency doubling indicates the successful generation of the biphotonic N00N-state. The simulations ((d) X, (e) XX and (f) T) are in very good agreement with the experimental results and can reproduce the phase dependency for all detection delays.

LOSS BUDGETING AND RESOURCE COUNTING

To describe the precision of the phase measurement in context of resource counting and loss budgeting, we make use of the theoretical description derived in *Thomas-Peter et al.* [11], which is based on the Fisher information and the (quantum) Cramér-Rao bound (QCRB) [12]. For evaluation and comparison we use the measurements conducted with photons emitted by the Trion state. In the following signal oscillations of the form $p = f(1 + C_N \cos(N\varphi))/2$ with a factor $f = \xi_p(\xi_i\xi_d)^N$, which is related to the Fisher information and describes the ratio of successful N00N state detection events with regard to the required input states, and the visibility contrast C will be considered.

Lossless system In the absence of losses ($f = 1$), the QCRB of N uncorrelated photons (classical light states) leads to the standard quantum limit (SQL), $\Delta\varphi \geq \Delta\varphi_{\mathrm{SQL}} = 1/\sqrt{N}$. For a quantum state such as the N00N state, the lower bound is given by the Heisenberg limit (HL), $\Delta\varphi = 1/NC \geq \Delta\varphi_{\mathrm{HL}} = 1/N$. By comparing the measured post selected (only successful events at zero detection delay) and the threshold visibility contrast C_{th} to surpass the SQL ($\Delta\varphi < \Delta\varphi_{\mathrm{SQL}}$) we obtain

$$\text{Required precision:} \quad C_{\mathrm{th}} = 0.71 \qquad < \qquad \text{Achieved precision:} \quad C_T = 0.87$$

Loss budgeting In the case off a lossy interferometer with transmissivity ξ_i and finite detector efficiencies ξ_d, the lower bound when using classical states is now given by the standard interferometric limit (SIL) [11, 13], $\Delta\varphi \geq \Delta\varphi_{\mathrm{SIL}} = 1/\sqrt{\xi_i\xi_d N}$. A N00N state on the other hand, is more vulnerable to losses which is expressed by the scaling of the transmissivity with ξ_i^N, leading to a QCRB of $\Delta\varphi \geq 1/\sqrt{(\xi_i\xi_d)^N NC}$. With the experimentally determined values $\xi_i = 0.90$ and $\xi_d = 0.45$ the required precision contrast of the SIL exceeds unity, which can not be outperformed, no matter which states were employed. Provided the use of state-of-the-art detectors with efficiencies of $\xi_d = 0.95$ [14], however, the SIL can be surpassed again by partially post selection of successful events, but including the above mentioned losses:

$$\text{Required precision:} \quad C_{\mathrm{th}} = 0.76 \qquad < \qquad \text{Achievable precision:} \quad C_T = 0.87$$

Resource counting In the context of resource counting, which is an important issue in biological sensing applications, where the sample may see only a limited amount of photons in total, the performance of a quantum light source is graded by the efficiency of state

generation. Every photon which does not contribute to the N00N state will nonetheless pass by the sample without leading to any gain in phase information. In this definition, the post selection process by taking into account only successful state generation events (coincidences at zero detection delay), is not valid. By including the state generation efficiency ξ_p, the QCRB is described by $\Delta\varphi \geq 1/\sqrt{\xi_p(\xi_i\xi_d)^N}NC$, whereas the classical SIL remains unchanged. The efficiency to generate a N00N state ξ_p with our approach is determined by three factors, namely the photon extraction efficiency $\epsilon_{\mathrm{ext}} \sim 0.01$ (this quantity corresponds to the heralding efficiency in heralded schemes, e.g., using parametric-down conversion sources), the generation method success rate $\epsilon_{\mathrm{m}} = 0.25$ (only in one out of for cases two consecutive emitted photons impinge on BS2′ from opposite sides) and the two-photon interference visibility $V_{\mathrm{HOM,T}} = 0.92$. The total generation efficiency is then given by $\xi_p = \epsilon_{\mathrm{ext}}^2\epsilon_{\mathrm{m}}V_{\mathrm{HOM,T}} \sim 2 \cdot 10^{-5}$, thus the limiting factor for super-sensitive measurements. To give an impression what could be possible with todays technology, we may assume, similar to the paragraph above, the state-of-the-art QD single-photon sources with $\epsilon_{\mathrm{ext}}^{\mathrm{opt}} \sim 0.80$ [15, 16], $\epsilon_{\mathrm{m}}^{\mathrm{opt}} = 1$ (by utilizing, e.g., a fast optical switch in the interferometer) and $V_{\mathrm{HOM}}^{\mathrm{opt}} = 0.99$ [7–9]. Thus, the generation efficiency would reach a value as high as $\xi_p^{\mathrm{opt}} = 0.63$ and therefore:

$$\text{Required precision:} \quad C_{\mathrm{th}} = 0.96 \qquad \sim \qquad \text{Achievable precision:} \quad C_{\mathrm{opt}} = 0.96$$

On the one hand, this result underlines the enormous demands put on source, setup and detector performance to reach quantum enhanced measurements with real-world sensors. On the other hand, the result implies, that with current technologies based on QD single-photon sources, this goal is come into reach and gives reason to hope for the realization in the near future.

DETERMINISTIC SINGLE-PHOTON SOURCES IN QUANTUM METROLOGY

Compared to probabilistic sources such as parametric down-conversion or four-wave-mixing techniques, deterministic single-photon sources can offer several advantages in optical quantum metrology schemes.

A major challenge in optical phase measurement schemes based on entanglement is to get the knowledge if or when a biphotonic N00N state has been successfully generated. While a deterministic source always produces one entangled photon pair at a time, for probabilistic

sources the creation time is entirely random. To overcome this problem, multiplexing and heralding schemes have been developed for the latter. However, these techniques involve a large overhead, unfavorable for practical applications, and additionally introduce loss channels, for instance in the heralding process, which have to be compensated.

Another important point may be the absolute N00N state detection rate. For a realistic sensing scheme, e.g., in biological sensing applications, the measurement has to performed fast. Recent promising works using cavities for efficient light extraction with resonantly driven QDs [7–9] demonstrated a state-of-the-art extraction efficiency of $\epsilon = 0.65$. Operating such a source at the highest possible repetition rate (lifetime of the emitter $\sim$ 500 ps) results in a rate of $7 \cdot 10^5$ coincidences per second, exceeding the highest reported value of 10^4 coincidences per second for Poissonian sources in [17] by nearly two orders of magnitude.

Concerning higher order N00N states ($N > 2$), non-classical N-photon states using N independently generated photons will also largely profit from on-demand sources due to an enhanced scaling behavior [18]. In the scheme presented in [18], the success probability p to generate a N00N state utilizing N independently but deterministically generated single-photons is given by $p(N) = 2N!/(2N)^N$. Probabilistically generated single-photons with a generation rate γ, however, will reduce the overall N00N state success probability drastically by factor of γ^N. This rapid decreases of success probability with increasing photon number reveals the need of highly efficient single-photon sources, particularly in this scheme.

* m.mueller@ihfg.uni-stuttgart.de

† p.michler@ihfg.uni-stuttgart.de

[1] S. Maier, P. Gold, A. Forchel, N. Gregersen, J. Mørk, S. Höfling, C. Schneider, and M. Kamp, Opt. Express **22**, 8136 (2014).

[2] K. Brunner, G. Abstreiter, G. Böhm, G. Tränkle, and G. Weimann, Phys. Rev. Lett. **73**, 1138 (1994).

[3] S. Stufler, P. Machnikowski, P. Ester, M. Bichler, V. M. Axt, T. Kuhn, and A. Zrenner, Phys. Rev. B **73**, 125304 (2006).

[4] H. Jayakumar, A. Predojević, T. Huber, T. Kauten, G. S. Solomon, and G. Weihs, Phys. Rev. Lett. **110**, 135505 (2013).

[5] M. Müller, S. Bounouar, K. D. Jöns, M. Glässl, and P. Michler, Nat. Photon. **8**, 224 (2014).

[6] Y.-M. He, Y. He, Y.-J. Wei, D. Wu, M. Atatüre, C. Schneider, S. Höfling, M. Kamp, C.-Y. Lu, and J.-W. Pan, Nat. Nanotechnol. **8**, 213 (2013).

[7] X. Ding, Y. He, Z.-C. Duan, N. Gregersen, M.-C. Chen, S. Unsleber, S. Maier, C. Schneider, M. Kamp, S. Höfling, C.-Y. Lu, and J.-W. Pan, Phys. Rev. Lett. **116**, 020401 (2016).

[8] N. Somaschi, V. Giesz, L. De Santis, J. C. Loredo, M. P. Almeida, G. Hornecker, S. L. Portalupi, T. Grange, C. Antón, J. Demory, C. Gómez, I. Sagnes, N. D. Lanzillotti-Kimura, A. Lemaítre, A. Auffeves, A. G. White, L. Lanco, and P. Senellart, Nat. Photon. **10**, 340 (2016).

[9] S. Unsleber, Y.-M. He, S. Gerhardt, S. Maier, C.-Y. Lu, J.-W. Pan, N. Gregersen, M. Kamp, C. Schneider, and S. Höfling, Opt. Express **24**, 8539 (2016).

[10] M. Kacprowicz, R. Demkowicz-Dobrzański, W. Wasilewski, K. Banaszek, and I. A. Walmsley, Nat. Photon. **4**, 357 (2010).

[11] N. Thomas-Peter, B. J. Smith, A. Datta, L. Zhang, U. Dorner, and I. A. Walmsley, Phys. Rev. Lett. **107**, 113603 (2011).

[12] S. L. Braunstein and C. M. Caves, Phys. Rev. Lett. **72**, 3439 (1994).

[13] U. Dorner, R. Demkowicz-Dobrzanski, B. J. Smith, J. S. Lundeen, W. Wasilewski, K. Banaszek, and I. A. Walmsley, Phys. Rev. Lett. **102**, 040403 (2009).

[14] A. E. Lita, A. J. Miller, and S. W. Nam, Opt. Express **16**, 3032 (2008).

[15] J. Claudon, J. Bleuse, N. S. Malik, M. Bazin, P. Jaffrennou, N. Gregersen, C. Sauvan, P. Lalanne, and J.-M. Gérard, Nat. Photon. **4**, 174 (2010).

[16] O. Gazzano, S. Michaelis de Vasconcellos, C. Arnold, A. Nowak, E. Galopin, I. Sagnes, L. Lanco, A. Lemaître, and P. Senellart, Nat. Commun. **4**, 1425 (2013).

[17] B. Bell, S. Kannan, A. McMillan, A. S. Clark, W. J. Wadsworth, and J. G. Rarity, Phys. Rev. Lett. **111**, 093603 (2013).

[18] H. F. Hofmann, Phys. Rev. A **70**, 023812 (2004).